Modeling and Visualization for a Pearl-Quality Evaluation Simulator

Noriko Nagata, Toshimasa Dobashi, Yoshitsugu Manabe,
Teruo Usami, *Member, IEEE,* and Seiji Inokuchi, *Member, IEEE*

Abstract—Visual simulation using CG and VR has attracted wide attention in the machine vision field. This paper proposes a method of modeling and visualizing pearls that will be the central technique of a pearl-quality evaluation simulator. Pearls manifest a very specific optical phenomenon that is not dependent on the direction of the light source. To investigate this feature, we propose a physical model, called an "illuminant model," for multilayer film interference considering the multiple reflection in spherical bodies. The rendering algorithm has been configured from such representations of physical characteristics as interference, mirroring, and texture, which correspond, respectively, to the sense of depth, brightness, and grain that are the main evaluation factors obtained from psychological experiments. Further, portions of photos of real pearls and the images generated by the present method were evaluated based on a scale of psychological evaluations of "pearl-like quality," demonstrating, thereby, that not merely the generated images as a whole, but the respective parts of images can present such a pearl-like quality.

Index Terms—Quality evaluation, physics-based modeling, multilayer film interference, psychological scaling, inspection, pearl.

———————————— ✦ ————————————

1 INTRODUCTION

V ISUAL simulation using computer graphics and virtual reality has come to be used recently in machine vision to enhance measurement and inspection systems [1], [2], [3]. This approach is an "analysis by synthesis" method which is employed to find the optimum inspection conditions and inspection criteria through the simulation of the item for inspection. It is considered to be an important technology which will meet the need to upgrade inspection systems and improve their accuracy.

In developing the pearl-quality evaluation system, the authors of this paper have, so far, made various analytical approaches, including factor analysis [4] and factor identification using neural networks [5], [6], and succeeded in deriving a detailed relationship between the physical information regarding pearls and their evaluation by human experts. In this paper, we describe a visual simulator which can form a virtual pearl sample in order to verify and correct the analytical results of the synthetic approach shown in Fig. 1.

Pearls are widely known as the "wonder of the Orient," and are remarkably popular as jewelry items. They also have the specific optical and structural features given below [7].

1) A pearl has a unique and lustrous iridescence with its multilayer, thin-film structure, due to its diverse optical behavior, such as refraction, interference, diffraction, and multiple reflection. Above all, the phenomenon of the hue distribution of the interference of light is extremely characteristic. It constantly shows a con-

centric change from the center of the sphere which does not depend on the direction of the light source.
2) A pearl is a natural substance whose film thickness and surface roughness are nonuniform, indicating natural irregularities and fluctuations.

The modeling and visualization of a pearl, a substance extremely interesting from the optical point of view, as was seen above, is, therefore, a worthwhile topic for investigation.

Several studies have, so far, been made concerning the simulation of the behavior of light, including the refraction of glass [8] and anisotropic substances [9], and the interference of a few layers of thin films [10], [11]. However, little attention has been paid to multilayer, thin-film interference. Moreover, an investigation of the optical phenomenon of pearl mica paint has been reported [12]; however, no such report has ever been made on actual pearls.

As for the visualization of natural objects, there have been many studies on clouds [13], fruit [14], and knitting yarn [15], for example. One thing common to these works is the use of a physical model which effectively adopts the individual features and functions of these objects, such as the factors related to their movement, growth, fluctuations, and texture.

The ultimate goal of this research is to clarify a pearl's inspection criteria by using various kinds of virtual sample, and collecting and analyzing the intuitive judgments of human experts. The evaluation of pearl quality is based on the intuition and experience of an expert, and is, therefore, delicate and vague. Hence, it is important that the intuitive judgment of the expert corresponds easily with the physical factors.

This paper proposes a pearl-generation algorithm based on a physical model which will become the central technique for the planned simulator [16]. In order to represent the specific hue distribution independently of the direction of the light source, we propose a physical model for multilayer thin-film interference in a spherical body, called an

————————————————
- *N. Nagata and T. Usami are with the Industrial Electronics & Systems Laboratory, Mitsubishi Electric Corporation, 8-1-1 Tsukaguchi-honmachi, Amagasaki, 661 Japan. E-mail: {nagata, usami}@con.sdl.melco.co.jp.*
- *T. Dobashi, Y. Manabe, and S. Inokuchi are with the Department of Systems Engineering, Osaka University, 1-3 Machikaneyama, Toyonaka, 560 Japan. E-mail: dobashi@inolab.sys.es.osaka-u.ac.jp, {manabe, inokuchi}@sys.es.osaka-u.ac.jp.*
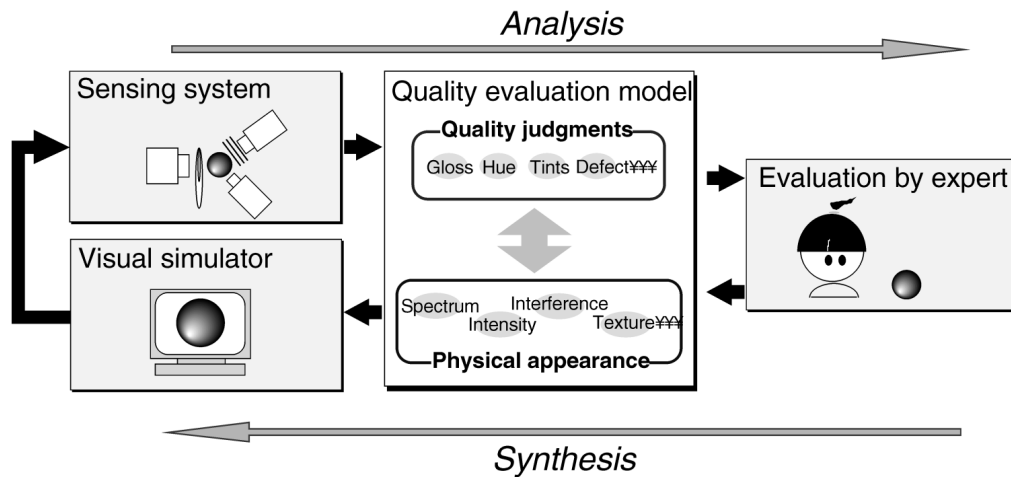
Fig. 1. The process of building up a pearl-quality evaluation system by analytical and synthesis approaches.

"illuminant model," which deals with each point in the layer as a point light source. Also, it was revealed in our previous study that the psychological factors in the quality evaluation of pearls include a sense of depth, brightness, and grain [4]. Therefore, the image-generating algorithm is configured from such representations of physical characteristics as interference, mirroring, and texture, which correspond with these three psychological factors. Furthermore, in the process of image generation, a psychological scale we call the "pearl-like quality" is configured from portions of photos of real pearls, which are then matched with pearl-like quality compositions of the corresponding portions of the generated images in order to evaluate them.

2 MODELING A PEARL

This section deals with the basic description of a pearl, namely, the physical models of multilayer thin-film interference and the interference light-calculation algorithm.

2.1 Physical Model of Multilayer Thin-Film Interference

A pearl is composed of a nucleus with a diameter of about 3 to 6 mm surrounded by nacreous layers 30 to 500 microns thick. The nacreous layers are formed of translucent films of 300 to 800 nm thick aragonite crystallized layers and less than 20 nm thick protein membranes alternatively deposited concentrically in 60 to 1,000 stacks. When the highly transparent crystallized layers are laminated uniformly, a unique lustrous iridescence appears due to interference and multiple reflection [7]. This phenomenon is regarded as multilayer thin-film interference caused by two kinds of optical film with different refractive indices [17].

The particular characteristic of the interference phenomenon of a pearl is the hue distribution of the interference color. Through the observation of a real pearl, we can see that the color fringe changes concentrically from the center of the sphere, and also can be observed on the opposite side to the light source, where light does not hit directly. In other words, the interference color of a pearl depends solely on the direction of the eyes, and not on the direction of the light source.

In normal thin-film interference, the color change of the interference light source largely depends on the direction of the light source. This is because the phase difference of two interference waves depends on the incident angle of the light. This phenomenon is seen in the shifting of the transmitted/reflected light spectrum of a narrow-band-pass filter or a multilayer thin-film coating to the short-wave side when the incident angle becomes larger. It can be easily observed that light changes color from green to blue to violet to red, etc., as a narrow-band-pass filter facing a light source is gradually inclined. Incidentally, a flat nacreous layer similar to that of a pearl, mother-of-pearl, is formed inside the shell of a pearl oyster, the mother shell of a pearl. In this case, however, the color changes either by shifting the eyes or by moving the light source. In other words, the color changes due to the incident angle, i.e., the direction of the light source. It can, therefore, be deduced that the hue distribution of the interference color of a pearl is an optical feature caused by the shape (spherical body) of the pearl.

In order to simulate this phenomenon, we propose a physical model of multilayer thin-film interference, called an "illuminant model," which pays careful attention to the multiple reflection of light inside a pearl, as shown in Fig. 2. Some of the light reaching the pearl surface goes inside the pearl, is repeatedly reflected and transmitted, and is propagated to the rear of the nucleus before being distributed over the whole nacreous layer. As a result, it appears as if each point in the layer had a point light source transmitting rays in all directions, with each ray causing local interference, as shown in Fig. 3. In other words, the light waves reflected on the boundary surfaces of each layer interfere with each other within the extremely short coherence distance of natural light. Here, as the phase difference of the reflected wave is determined by the angle between the reflected wave and the nacreous layer, the power spectrum of the interference light depends only on the refractive angle. As the interference takes place everywhere in the nacreous layer, each interference ray is propagated in all directions outside the pearl. Taking account of only the interference light waves propagated in the direction of viewpoints (a) and (b) in Fig. 2, the light from each point on the concentric circle is the interference light
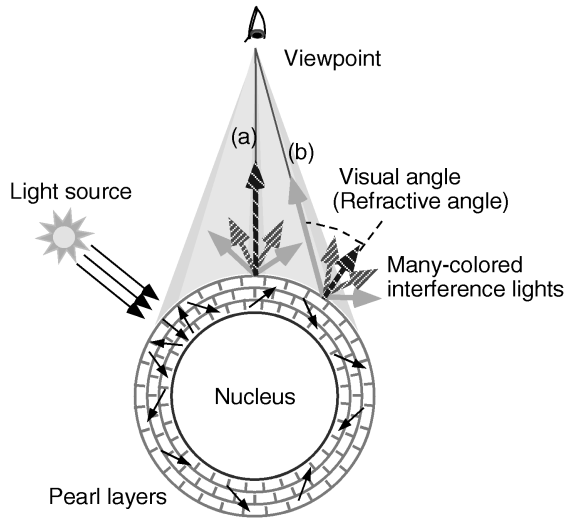
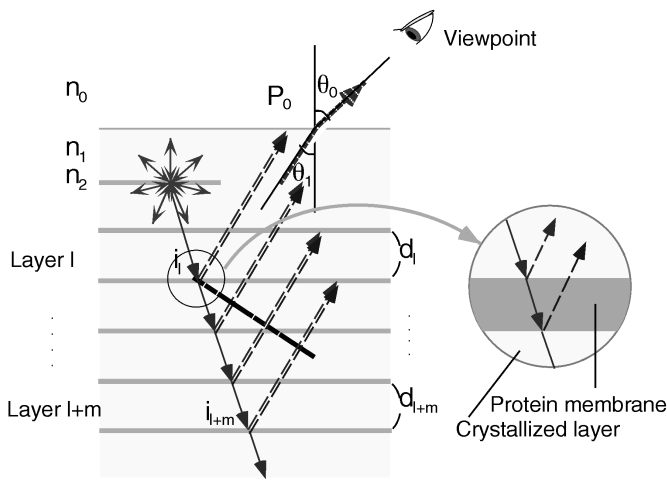Fig. 2. A physical model of the multilayer thin films of a pearl.

Fig. 3. The interference of incident light in the nacreous layer.

propagated with the same angle of refraction, so that the phase difference, i.e., the spectrum distribution, must be equivalent. It follows from this that the independence of the interference light color from the direction of the light source and its change in concentric form can thus be explained.

2.2 Calculation Algorithm of Interference Light

The power spectrum of interference light is calculated on the basis of the model. Fig. 3 shows the structure of the nacreous layers and the behavior of the interference. The multilayer structure is composed of L layers, each alternately composed of stacks of crystallized nacreous layers of thickness d_l and of thin protein membranes. Here n_0, n_1, n_2 are the refractive indices for the air spaces, crystallized layers, and protein membranes, respectively.

The flow of the interference light calculation is given in Fig. 4. The flow of the algorithm in a broad sense is described first in compliance with Fig. 4. First, the crystallized layer film thickness column is generated, followed by casting a ray from the viewpoint to calculate the intersection with the pearl. The incident angle, reflectance, and transmittance of all intersecting rays are calculated before making interference
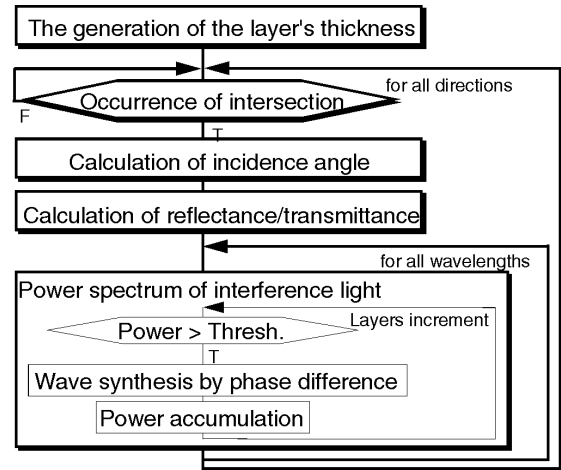

Fig. 4. A flowchart for the simulation of interference light.

calculations from the outer layer to the inner layer of the nacreous layer for all visible wavelength bands in order to obtain the spectral power. The methods of calculation are given below.

2.2.1 Generation of Crystallized Layer Film Thickness Column

As mentioned above, a pearl is a natural object, so that the structure of its layers is not uniform. The growth of a pearl corresponds to the changes in the season, with the pearl having a thicker and larger number of films, but lower transparency, in the summer, while, in autumn and winter, crystallized films less than 500 nm thick with high transparency are obtained. It is for this reason that pearls are harvested around December [7]. Hence, a film thickness generation method which imitates the growing process of a pearl can make it possible to evaluate or represent a natural pearl.

As a method of generating the crystallized layer thickness column d_l, the thickness (400-700 nm) per layer and the number of films (1-3) per day are expressed by the normal distribution functions, and the thickness and number of films are further varied by using random numbers. The parameters of these functions are determined by the growth curve of the pearl [7]. The thickness of the protein membrane is set to a constant 20 nm.

2.2.2 Calculation of Incident Angle

The interference light calculation is carried out only for light which reaches the viewpoint. The light arriving at the viewpoint from point P_0 on the pearl surface is considered as follows: First, a single ray in a nacreous layer is reflected by the l layer to the $l + m$ layer, and divided into the coherent rays i_l to i_{l+m}, which later interfere with each other. Next, the interference light enters at P_0 from the nacreous layer with a refractive index n_1 to the air space of refractive index n_0 at the angle of incidence θ_1, and refracts at the angle θ_0. Therefore, from the viewpoint and the position of point P_0, the refractive angle θ_0, in other words, the visual angle between the eye direction and the surface normal, is determined uniquely, and the angle of incidence θ_1 is calculated from Snell's law given by the following formula;

$$\frac{\sin \theta_1}{n_1} = \frac{\sin \theta_0}{n_0}. \tag{1}$$

2.2.3 Calculation of Reflectance/Transmittance

The reflectance or transmittance is essentially determined by the refractive index of an object and the incident angle of light, and can be calculated using Fresnel's equations [17]. The larger the difference in the refractive index between two objects, the greater the reflectance is changed due to the incident angle. The reflectance to be considered here is the reflectance between the crystallized layer and the air space, and the reflectance between the crystallized layer and the protein membrane.

First, the energy reflectance R_1 ("reflectance") and the energy transmittance T_1 ("transmittance") when the light enters from the crystallized layer to the air space can be calculated by using Fresnel's equations in the following manner.

$$R_1 = \frac{1}{2}\left(\left|r_1^p\right|^2 + \left|r_1^s\right|^2\right), \tag{2}$$

$$T_1 = 1 - R_1, \tag{3}$$

where:

$$r_1^p = \frac{n_1 \cos\theta_0 - n_0 \cos\theta_1}{n_1 \cos\theta_0 + n_0 \cos\theta_1}, r_1^s = \frac{n_1 \cos\theta_1 - n_0 \cos\theta_0}{n_1 \cos\theta_1 + n_0 \cos\theta_0}.$$

Here, r_1^p, r_1^s are the amplitude reflectances for p-polarized light and for s-polarized light, respectively. It is known that light can be separated into two components, p-polarized light and s-polarized light, the directions of amplitude of which are orthogonal to each other, and, in natural light, both these polarizations are contained equally. Therefore, the values of R_1 and T_1 are obtained in the above manner. Fig. 5 shows the relationship between the incident angle θ_1 and the reflectance R_1. It indicates that the reflectance increases when the visual angle is large, with the interference color transmittance, i.e., intensity, becoming smaller toward the periphery of the pearl. In this calculation, the refractive index n_1 is calculated by taking the C-axis refractive index of aragonite crystal as 1.53 and n_0 as 1.0. The C-axis, which is one of the three orthogonal crystallographic axes of the crystal, runs parallel with the surface normal of the nacreous layer.

Next, the reflectance R_2 and the transmittance T_2 between the crystallized layer and the protein membrane are also calculated in the same manner. Although the refractive index n_2 of the protein membrane is not known, it is regarded as 1.43. The reasoning behind this value is that n_2 is smaller than n_1 since the multiple reflection more likely takes place in the aragonite crystallized layer, not in the protein membrane, and that the nucleus inside can be seen when the layer is thin (60-100 layers), thus, the transmittance is quite high; in other words, there is little difference between n_1 and n_2.

2.2.4 Calculation of the Power Spectrum

When we consider the light transmitted from the outer to the inner layer with the incident angle calculated in Section 2.2.2., the reflected light waves are combined by calculating the phase differences between the waves. The phase difference ξ, due to the difference in the optical path between the reflected lights at the l layer and the $l + k$ layer, is computable for the wavelength λ with the following formula.

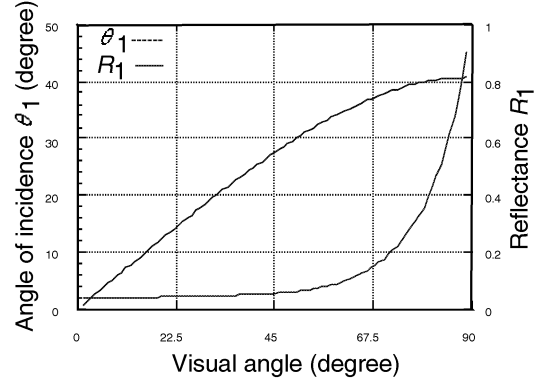$$\xi = 4\pi \sum_{i=l+1}^{k} d_i\left(n_1/n_0\right)\cos\theta_1/\lambda. \tag{4}$$

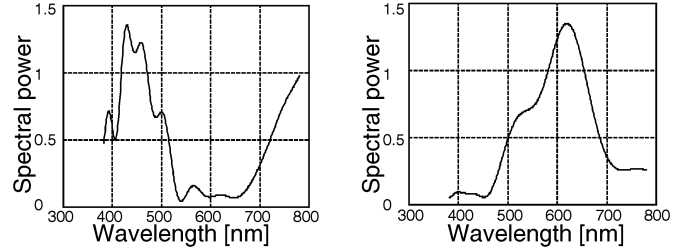Fig. 5. Angle of incidence and reflectance by visual angle.

Fig. 6. Spectral power distribution of interference light.

The resultant waves are calculated by applying (4) and the reflectance and transmittance obtained in Section 2.2.3. The reflected waves above and under the protein membrane are also combined similarly to substitute n_1 and n_2 to (4). The calculation is done first by finding the combined waves above and under the protein membrane, and then by further adding the combined waves using (4). These calculations are made for each visible wavelength band (380 to 780 nm).

The interference calculation, starting from the first layer until the optical path difference reaches the coherence distance of natural light, is taken as one cycle of interference. The coherence distance here is regarded as 5 microns. Calculations are further made through the succeeding layers until the light intensity fails to conform to the threshold value to obtain the spectral power. Calculations are stopped when the final light intensity reaches the threshold value of 0.05.

The interference light spectral power distribution at two given points is shown in Fig. 6, indicating the flat spectrum distribution of white light being changed due to interference. Further, these correspond to the directions of viewpoints (a) and (b) in Fig. 2, revealing that the spectrum distribution differs according to the visual angle.

As for the absorption for each layer, it is not considered here because it is very slight, but is dealt with as an object color in a later section.

3 GENERATION OF A PEARL IMAGE

The interference light spectrum obtained is converted into an RGB image, and is combined with the components of specular reflection and diffuse reflection, obtained through calculation, to generate the pearl image. In order to evaluate the pearl quality in particular, the three major psychological factors, sense of depth (layer uniformity), sense of bright-

ness (surface reflection), and sense of grain (surface uniformity), are employed.

3.1 Representation of the Sense of Depth Due to Interference Light

The sense of depth corresponds to the expressions "thickly rolled," "strong tint," obtained through the questionnaires given to human experts, and is considered to be related mainly to the intensity of interference color [4]. The diffuse reflection, as well as the film thickness and the number of films, are considered to be the parameters likely to change the sense of depth, which is regarded as a function of diffusion in a normal rendering model. Hence, the sense of depth is expressed by calculating the diffuse-reflected light by using the object color of the pearl, and then varying the mixing ratio with the interference light. Fig. 7a shows the image of the diffuse reflected light. The color of the light is calculated by using the spectrum obtained by physically measuring a pearl, by which absorption of the nacreous layer is also considered. Fig. 7b shows an example of the image of the interference light component, where the bluish rainbow color, considered to be the most beautiful of the pearl interference lights, can be clearly observed.

3.2 Representation of the Sense of Brightness Due to Mirroring

Careful observation of a pearl shows that the background and the illumination of the circumference are mirrored well on the surface of the pearl. This was expressed by the experts during interviews as "mirroring one's face well" [4]. Furthermore, since the mirroring is known to play an important role in the sense of quality of a transparent object, it is expected to be an effective method of expressing the sense of brightness. To represent the difference in mirroring due to surface variations, the Cook-Torrance model [18] is used to compute the surface reflection of the light source. This model has a geometric attenuation factor caused by the surface microfacets, and the microfacets' slope D is given by the Beckmann function, as in the following formula;

$$D = \frac{\exp\left(-\left(\tan \delta / m\right)^2\right)}{m^2 \cos^4 \delta}. \tag{5}$$

Here, δ is the angle between the surface normal and the microfacet's normal. Plural Ds are calculated by varying the value m. The specular reflections at the inner layers are also considered. The ray tracing method is used to mirror the surrounding object, with the attenuation of the light intensity for mirroring with the increase of distance between the nacreous surface and the object. An example of the image of the mirrored light source and the table is given in Fig. 7c.

3.3 Representation of the Sense of Grain Due to Texture

Unique textures expressed by "zara zara" (rough) or "mera mera" (flame-like) are observed on the surface of a pearl. These textures are caused by the irregular-striped patterns on the surface of a pearl, composed of the stacks of stepped crystallized layers, and the irregular orientation of crystals inside the pearl. As a simple method of generating such

(a) A diffuse image   (b) An interference component

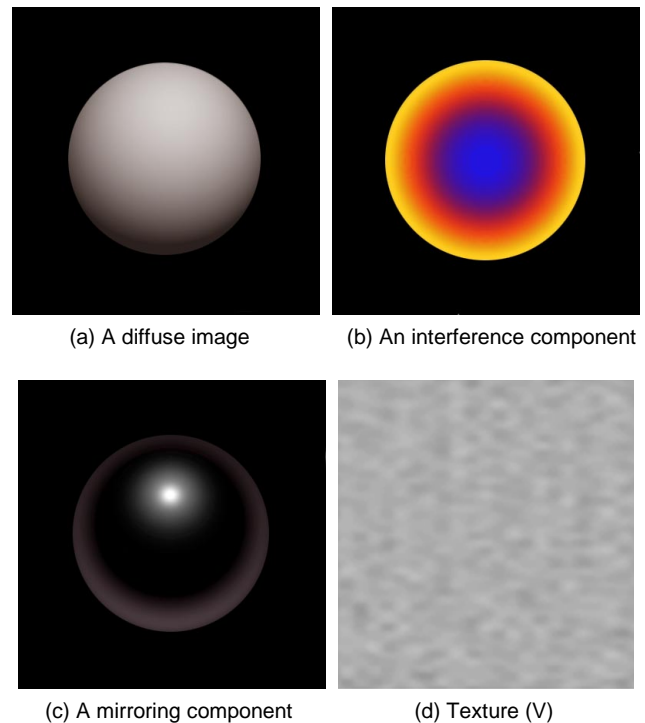(c) A mirroring component   (d) Texture (V)

Fig. 7. Components of a synthesized image.

textures, the high frequency component, extracted from the photograph of a real pearl by using two-dimensional FFT/inverse FFT, is mapped on the nacreous surface. In order to enable an intuitive understanding and to allow the easy setting of parameters, the RGB of the image is converted into the Munsell color system (HVC space), and the texture factors of hue (H), value (V), and chroma (C) are used.

The RGB image of the partial photograph of a pearl, used in Section 4, is converted into an HVC image. After the Hunning window function [19] is then applied to each image, the power spectrum by using two-dimensional FFT is obtained. The power spectrum is passed through the band-pass filter, then undergoes inverse FFT to obtain the texture image of the HVC space. The example of value (V) texture (with expanded spatial and density scales) is shown in Fig. 7d.

3.4 Example of Synthesis

The generated component images are synthesized as follows. The power spectrum of light is converted into an HVC image once, so that the mapping texture has an appropriate weight, before being converted into an RGB image. As a result of trying to add each of the factors to component images with various weights, we found it best to adopt H and C factors for the diffuse reflection image, and V for the mirroring image with the weight being proportional to the values of the image established by experience.

Examples of synthesis using this method are given in Fig. 8. The interference component and mirroring component are added to the diffuse image. The light source makes an angle of 45 degrees with the view direction, and the interference color is calculated independently of the direction of the light source. However, a contradiction is not felt, and a realistic pearl interference can be represented. A sense of brightness and transparency is also expressed by mirroring.
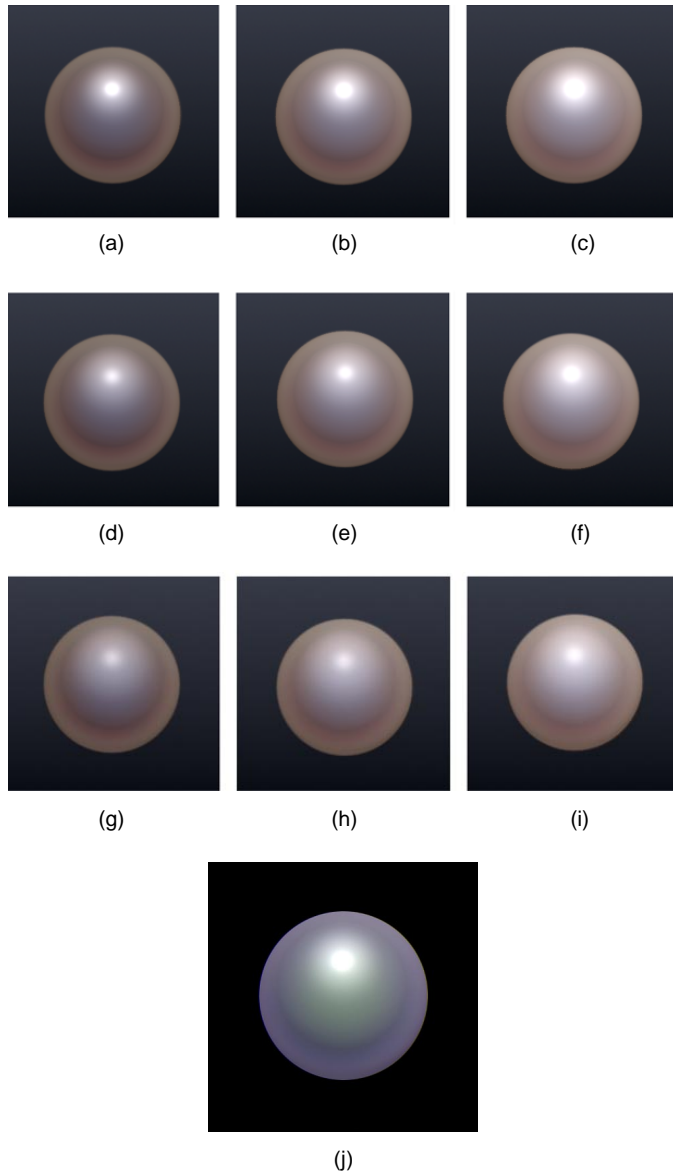
(a)   (b)   (c)

(d)   (e)   (f)

(g)   (h)   (i)

(j)

Fig. 8. Synthesized images.

TABLE 1
PARAMETERS

	Mixing Ratio			m (in Beckmann function)
	Diffuse component	Interference component	Mirroring component	
(a)	43.0	7.0	50.0	0.20
(b)	49.5	6.5	44.0	0.20
(c)	54.0	6.0	40.0	0.20
(d)	43.0	7.0	50.0	0.25
(e)	49.5	6.5	44.0	0.25
(f)	54.0	6.0	40.0	0.25
(g)	43.0	7.0	50.0	0.30
(h)	49.5	6.5	44.0	0.30
(i)	54.0	6.0	40.0	0.30

(a) synthesized pearl   (b) real pearl

Fig. 9. Superimposition of a synthesized image on a photo of real pearls.

source. The LUT has RGB values for every one degree of the visual angle, and in the generation of an image of an interference component, the RGB values of the visual angle are calculated by using linear interpolation between degrees. The LUT generation takes about three minutes, but, once the table has been made, the image generation can be done in the order of several seconds for a 200 * 200 resolution image.

4 PSYCHOLOGICAL SCALING OF "PEARL-LIKE" QUALITY

So far, there is hardly any general method of making a quantitative evaluation of a CG-expressed image. In this section, we would like to try the evaluation of synthesized images by using the expression "-like quality."

The CG representation method can be broadly divided into two types: One is to bring the image infinitely close to the real object by using physical phenomenon and a mathematical model, and the other is to make the object more real than itself by effectively extracting (and sometimes even by exaggerating) the modeling features and movements, as in the case of deformation [20] in a picture or portrait. These two methods can be summarized as follows:

1) Expression of reality,
2) Expression of abstraction.

In consideration of the various restrictions, such as the characteristics of the display device, calculation cost, etc., the simulation of pearls can be carried out by making an abstract evaluation of the pearl features and by emphasizing the relevant factors, while utilizing a realistic expression based
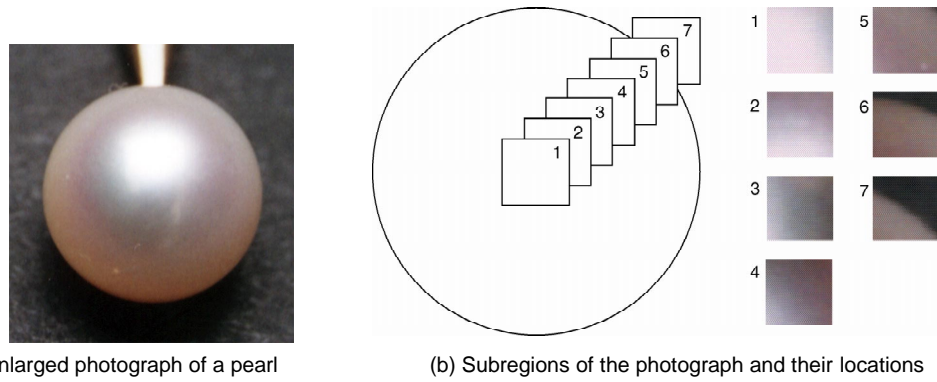
By varying the mixing ratio of the diffuse component and the interference image, the difference in the sense of depth is shown. In Figs. 8a to 8i, the more to the left an image is the stronger is the sense of depth. By varying the parameters of the mirroring component, the difference in brightness is shown. The higher images are brighter. The values of each parameters are shown in Table 1. Fig. 8j shows the texture added to Fig. 8a. Slight as the color change is, it is confirmed by experts that the change improves the sense of grain and reality on the surface of the pearl.

To allow a comparison of our result with real pearls, the superimposition of the synthesized image on a photo of real pearls is shown in Fig. 9. It follows, therefore, that this method can effectively represent the optical phenomena of pearls.

The generation of computations without interference takes a few seconds on an SGI Power Onyx graphics workstation. As for the interference component, the LUT (lookup table) of the color changed by the visual angle is used because of its independence from the direction of the light

(a) An enlarged photograph of a pearl (b) Subregions of the photograph and their locations

Fig. 10. Photographs of a pearl.

TABLE 2
SCALE DISTANCE MATRIX ON "PEARL-LIKE QUALITY"

	1	2	3	4	5	6	7	Total	Average
1	0.000	−0.739	0.643	−0.050	0.305	0.706	1.080	1.945	0.278
2	0.739	0.000	0.583	0.498	1.227	1.282	1.341	5.670	0.810
3	−0.643	−0.583	0.000	0.385	0.806	1.175	1.126	2.266	0.324
4	0.050	−0.498	−0.385	0.000	1.080	1.405	1.282	2.934	0.419
5	−0.305	−1.227	−0.806	−1.080	0.000	0.706	0.553	−2.159	−0.308
6	−0.706	−1.282	−1.175	−1.405	−0.706	0.000	0.915	−4.359	−0.623
7	−1.080	−1.341	−1.126	−1.282	−0.553	−0.915	0.000	−6.297	−0.900

on a physical model, to make the expression closer to reality. Therefore, we examined this abstract-like quality closely.

First, in order to learn what kind of spatial pattern a person senses as a pearl, psychological experiments were carried out generating the pearl images using the key words pearl-like quality. Thurstone's method of paired comparisons [21], a rating method to quantify subjective judgment in the sensory evaluation field, was used for nonexperts in carrying out a rating experiment to construct a psychological scale of pearl-like quality. Second, the synthesized pearl images are evaluated using the same method of psychological evaluation by means of the pearl-like quality scale, and then compared with the photographs.

4.1 Evaluation of a Real Photograph of Pearl

In order to clarify what property is dominant for the pearl-like quality among specular reflectance, interference color, shape of pearl, etc., seven kinds of subregion with different characteristics were cut from an enlarged photograph of a pearl, as shown in Fig. 10. Next, 21 samples for evaluation, each consisting of two arbitrary subregions, were made.

A total of 103 university students, mainly majoring in science, were asked to make evaluations as to "which sample has the more pearl-like quality." For comparison, two rating cases were adopted: before and after observing a real pearl.

The scale-distance matrix due to the paired comparison method and the psychological scale values are shown, respectively, in Table 2 and Fig. 11, with photographs one to seven indicating the order from the center of a pearl. Further, the psychological scale values obtained before and after showing the real pearl to men and women are shown in Fig. 12. The following results were obtained from this experiment.

1) The results on the whole, show that it was felt that the most pearl-like photograph was the one containing both specular reflections and interference colors (Photo 2). It was followed by the photograph with interference colors only (Photo 4) and the photograph containing specular reflections only (Photo 1). The photographs which included profiles, on the other hand, were given poor ratings for pearl-like quality (Photos 5, 6, and 7).

2) The distances in the psychological scale values between the groups of pearl-like photographs (Photos 1, 2, 3, and 4) and nonpearl-like photographs (Photos 5, 6, and 7) were found to be larger, comparing the dispersion in the groups, for the case when real pearls had been observed than when they had not. Similarly, women, normally more familiar with pearls, apparently have a wider psychological scale distance than men. Since the populations of these values are not equivalent, it is not possible to make a simple comparison between these psychological scale values. However, these values, if regarded as the relative distance of dispersion, can evidently be taken as the scale for pearl-like quality.

These results thus indicate that a common psychological scale of pearl-like quality also exists among nonexpert people. The sense of pearl-like quality depends on factors related to specular reflections and interference colors. It is considered that this sense corresponds to "teri" and "maki," the technical terms implying the luster and interference color characteristic of a pearl, and that a common sense of what a pearl is exists between experts and nonexperts. It has also become clear that the profile of a pearl, i.e., the configurative factor, is of little influence on the pearl-like quality.
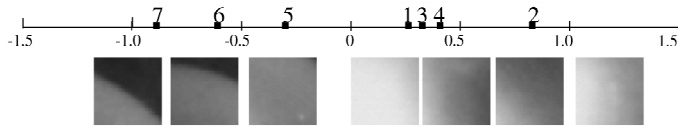
Fig. 11. A psychological scale of "pearl-like quality"—photograph—(103 subjects).
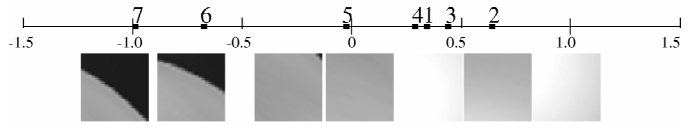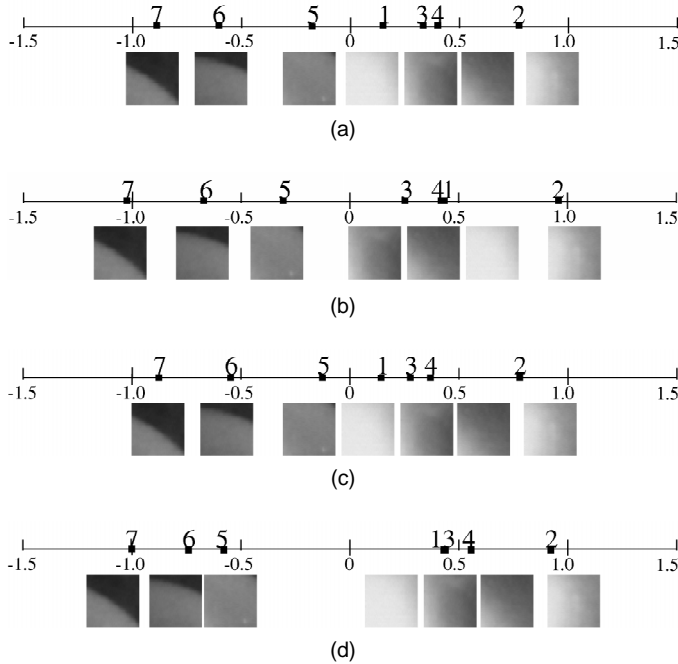

(a)

(b)

(c)

(d)

Fig. 12. Comparison of psychological scales. (a) Before observing a real pearl (63 subjects). (b) After observing a real pearl (40 subjects). (c) Men (61 subjects). (d) Women (42 subjects).

4.2 Evaluation of a Synthesized Image

Seven kinds of subregions were cut from the 400 * 400 synthesized image in the same manner as in Fig. 10 as samples for evaluation. The resolution of the image is the same as that of a photograph, which is thought to be enough for this test. The reason is that a 400 * 400 image of a pearl (about 7 mm in diameter) has information corresponding to 1,450 dpi, which seems to be quite enough for that of natural images, even if the image is enlarged seven times. In addition, from the viewpoint of comparison, a 400 * 400 image is sufficient, because our objectives are not graded absolutely, but are relatively compared.

A total of 50 university students were asked to evaluate the samples on the basis of their pearl-like quality.

The psychological scale values due to the paired comparison method are given in Fig. 13. As compared with the order of scale values obtained from the photographs, the order is the same except for image number 4, which is two ranks down. No change in order is seen in the other samples, so that the synthesized images on the whole do give the features of a real pearl. The reason for the low ranking of image number 4 seems to be that the smooth change in color in images number 1 and number 3 causes the evaluation of its pearl-like quality to become relatively weak. Furthermore, image number 2, evaluated as the most pearl-like, does not change its rank, but has a poorer

Fig. 13. A psychological scale of "pearl-like quality"—synthesized image—(50 subjects).

evaluation. This is attributed to the conspicuous roughness of the image. Image number 5, on the contrary, has a higher evaluation, because its color change is smoother than the photograph.

It can, therefore, be deduced that the synthesized images can give not only entire, but also partial representations of pearl-like quality. Also, the pearl-like quality involves smoothness, particularly the smoothness in color change.

5 CONCLUSION

We have proposed a representation technique for pearls on the basis of a physical model and a psychological evaluation in building up a visual simulator for pearls. This technique uses the illuminant model, which is a physical model of multilayer thin film interference, where only the light reaching a viewpoint is taken into account, in order to represent the specific color distribution, which is independent of the direction of the light source. Furthermore, the image synthesis algorithm is composed of the three major physical factors, namely, interference, mirroring, and texture, allowing the effective representation of a pearl. The parameters here are determined on the basis of experience, but the representation has been found to be more than satisfactory for multilayer thin-film interference which has, so far, not been tried in the field of CG. This technique will also be able to be applied to the design of inspection systems. Taking a concrete example, the color or the spectrum, the position, and the type, such as defused or direct, of a light source and reflectors can be compared and determined on the basis of this simulation. The specification of the system will be selected flexibly, depending upon the kind of pearls under inspection in a future project of ours.

By using a psychological scale of pearl-like quality, we next evaluated the photographs of a real pearl and synthesized images. The results show that a synthesized image can make a partial as well as a total simulation of the pearl-like quality. Furthermore, essential information has been acquired for representing real pearls, such as, the pearl-like quality is a psychological scale common to both experts and nonexperts, which is caused by the luster and interference color, and is influenced by a smooth color variation. It is expected that this information can be used also in image generation to reduce the computing time by making a coarse calculation of factors not contributing to pearl-like quality.

However, the method needs further improvements from the standpoint of a photorealistic representation of pearls. Some experts pointed out the lack of the sense of brightness in the synthesized images. In the representation of mirroring, we would like to work on a physical model where the

surface roughness and the spread or blur of light are taken into account. As for the texture, the introduction of chaos modeling is now being considered for representation of the dynamic fluctuation, because the texture of a pearl surface could be generated on the basis of the Chaotic generation model from the observation of a microscopic view of the pearl surface.

In the future, we plan to study the correspondence of the psychological and physical factors of the inspectors on the basis of this model. We also plan to select the physical parameters that could contribute to the pearl-like quality.

REFERENCES

[1] J.K. Kawai, J.S. Painter, and M.F. Cohen "Radioptimization—Goal Based Rendering," *Proc. Computer Graphics Ann. Conf. Series* (*SIGGRAPH '93*), pp. 147-154, Aug. 1993.
[2] K. Takamoto, M. Ito, A. Fukui, K. Takada, and K. Nishii, "Detection of Micro Cracks on Ceramic Devices*," Proc. SICE Sensing Forum*, no. 12, pp. 85-90, 1995.
[3] N. Chiba, Y. Okuda, F. Yasutomi, H. Kawata, and H. Tomita, "Specification of Image Features for the Sensory Inspection by Limit Samples," *Trans. IEE Japan*, vol. 116-D, no. 7, pp. 743-748, 1996.
[4] N. Nagata, M. Kamei, M. Akane, and H. Nakajima, "Development of a Pearl Quality Evaluation System Based on an Instrumentation of 'Kansei,'" *Trans. IEE Japan*, vol. 112-C, no. 2, 1992.
[5] N. Nagata, M. Kamei, and T. Usami, "Transferring Human Sensibilities to Machines—Sensitivity Analysis of Layered Neural Networks and Its Application to Pearl Color Evaluation," *Proc. IAPR Workshop Machine Vision Applications*, pp. 528-531, 1994.
[6] N. Nagata, M. Kamei, and T. Usami, "Factors Identification Using Sensitivity of Layered Neural Networks and Its Application to Pearl Color Evaluation," *Trans. IEE Japan*, vol. 116-C, no. 5, pp. 556-562, 1996.
[7] K. Wada, "Pearl," The National Jewelry Assoc., 1982.
[8] T. Yasuda, S. Yokoi, J. Toriwaki, S. Tsuruoka, and Y. Miyake, "An Improved Ray Tracing Algorithm for Rendering Transparent Objects," *Trans. Information Processing Soc. of Japan,* vol. 25, no. 6, pp. 953-959, 1984.
[9] P. Poulin and A. Fournier, "A Model for Anisotropic Reflection," *Computer Graphics*, vol. 24, no. 4, pp. 273-282, 1990.
[10] P. Hanrahan and W. Krueger, "Reflection from Layered Surfaces Due to Subsurface Scattering," *Proc. Computer Graphics Ann. Conf. Series (SIGGRAPH '94)*, pp. 213-220, 1994.
[11] J. Dorsey and P. Hanrahan, "Modeling and Rendering of Metallic Patinas," *Proc. Computer Graphics Ann. Conf. Series* (*SIGGRAPH '96*), pp. 387-396, 1996.
[12] J.S. Gondek, G.W. Meyer, and J.G. Newman, "Wavelength Dependent Reflectance Functions," *Proc. Computer Graphics Ann. Conf. Series (SIGGRAPH '94)*, pp. 213-220, 1994.
[13] J.T. Kajiya and B.P. Von Herzen, "Ray Tracing Volume Densities," *Proc. Computer Graphics* (*SIGGRAPH '84*), vol. 18, no. 3, pp. 165-174, July 1984.
[14] S. Tokai, M. Miyagi, T. Yasuda, S. Yokoi, and J. Toriwaki, "A Method for Rendering Citrus Fruits with Computer Graphics," *Trans. Institute of Electronics, Information and Communication Engineers*, vol. J76-D-2, no. 8, pp. 1,746-1,754, 1993.
[15] E. Groller, R.T. Rau, and W. Straber, "Modeling and Visualization of Knitwear," *IEEE Trans. Visualization and Computer Graphics*, vol. 1, no. 4, pp. 302-310, 1995.
[16] N. Nagata, T. Usami, Y. Manabe, and S. Inokuchi, "A Modeling and Rendering of Pearl for Quality Evaluation with Visual Simulator," *Trans. IEICE*, vol. J80-D-2, no.1, pp. 206-214, 1997.
[17] H.A. Macleod, *Thin-Film Optical Filters*. Techno House, 1986.
[18] R.L. Cook and K.E. Torrance, "A Reflectance Model for Computer Graphics," *ACM Trans. Graphics*, vol. 1, no. 1, pp. 7-24, Jan. 1982.
[19] F.J. Harris, "On the Use of Windows for Harmonic Analysis with the Discrete Fourier Transform," *Proc. IEEE*, vol. 66, no. 1, pp. 51-83, 1978.
[20] K. Murakami, H. Koshimizu, A. Nakayama, and T. Fukumura, "On the Facial Caricaturing System PICASSO Using Visual Illusion," *Trans. ICSJ*, vol. 34, no. 10, pp. 2,106-2,115, 1993.
[21] H. Harashima and S. Inokuchi, *Kansei Information Processing*. Ohmsha Ltd., 1994.
[22] K.E. Torrance and E.M. Sparrow "Theory for Off-Specular Reflection from Roughened Surfaces," J. Optical *Soc. Am.*, vol. 54, no. 91, pp. 1,105-1,114, 1967.

Noriko Nagata received the BS degree in mathematics from Kyoto University in 1983 and the PhD degree in systems engineering from Osaka University in 1996. Since 1983, she has been a researcher at the Industrial Electronics and Systems Laboratory of Mitsubishi Electric Corporation. Her research interests are mainly in the application of image analysis and synthesis, knowledge engineering, and Kansei information processing to industrial inspection.

Toshimasa Dobashi received the BS degree in engineering from Department of Systems Engineering, Osaka University. He is currently a second year MS student in physical science courses, Osaka University. His interests include physics-based rendering and computer graphics.
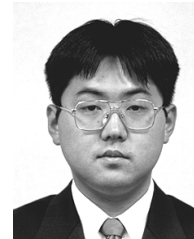
Yoshitsugu Manabe graduated in 1991 from the Department of Control Engineering, Faculty of Engineering Science, Osaka University, where he obtained a PhD in engineering degree in 1995. He was then appointed a research associate in the Department of Systems Engineering at Osaka University. He is engaged in research on color image processing and recognition.

Teruo Usami received the BS and MS degrees in applied physics from Osaka City University in 1971 and 1973, respectively. In 1973, he joined the Industrial Electronics and Systems Laboratory of Mitsubishi Electric Corporation, and, currently, he is a manager of the Sensing Systems Department. His research interests include diagnosis and inspection for plant systems.

Seiji Inokuchi graduated from the Department of Electrical Engineering, Osaka University in 1962, and received the MS and PhD degrees from Osaka University in 1964 and 1969, respectively. In 1965, he joined the Department of Control Engineering, the Faculty of Engineering Science, Osaka University, as an assistant professor, and, currently, he is a professor in the Department of Systems Engineering. He holds the post of project leader in LIST (Laboratories of Image Information Science and Technologies) concurrently. His main research interests include pattern measurement and recognition, 3D image processing, acoustic signal processing, and Kansei information processing. He is the author of *Three-Dimensional Image Measurement*, *Science of Sounds*, and *Kansei Information Processing*, written in Japanese.